Investigation of magnetic phase transition and magnetocaloric effect of (Ni,Co)-Mn-Al melt-spun ribbons

Yen Nguyen[1,*], *Mai* Nguyen [4], *Quang* Vu[2,3], *Thanh* Pham[1,2], *Victor* Koledov[5], *Alexander* Kamantsev[5], *Alexey* Mashirov[5], *Thanh* Tran[1,6], *Hau* Kieu[6], *Yu* Seong[6], and *Dan* Nguyen[1]

[1] Institute of Materials Science, Vietnam Academy of Science and Technology, 18 Hoang Quoc Viet, Ha Noi, Viet Nam
[2] Graduate University of Science and Technology, Vietnam Academy of Science and Technology, 18 Hoang Quoc Viet, Ha Noi, Viet Nam
[3] Faculty of Physics, Hanoi Pedagogical University 2, 32 Nguyen Van Linh, Vinh Phuc, Vietnam
[4] Faculty of Physics, VNU University of Science, 334 Nguyen Trai, Ha Noi, Viet Nam
[5] Kotelnikov Institute of Radio-engineering and Electronics of RAS, Moscow, Russia
[6] Department of Physics, Chungbuk National University, Cheongju 361 - 763, South Korea

Abstract. Magnetic phase transition, magnetocaloric effect and critical parameters of $Ni_{50-x}Co_xMn_{50-y}Al_y$ (x = 5 and 10; y = 17, 18 and 19) rapidly quenched ribbons have been studied. X-ray diffraction patterns exhibit a coexistence of the $L2_1$ and $10M$ crystalline phases of the ribbons. Magnetization measurements show that all the samples behave as soft magnetic materials with a low coercive force less than 60 Oe. The shape of thermomagnetization curves considerably depends on Co and Al concentrations. The Curie temperature (T_C) of the alloy ribbons strongly increases with increasing the Co concentration and slightly decreases with increasing the Al concentration. The $Ni_{45}Co_5Mn_{31}Al_{19}$ and $Ni_{40}Co_{10}Mn_{33}Al_{17}$ ribbons reveal both the positive and negative magnetocaloric effects. Under magnetic field change (ΔH) of 13.5 kOe, the maximum magnetic entropy change ($|\Delta S_m|_{max}$) of the $Ni_{45}Co_5Mn_{31}Al_{19}$ ribbon is about 2 and -1 $J \cdot kg^{-1} \cdot K^{-1}$ for negative and positive magnetocaloric effects, respectively. Basing on Arrott - Noakes and Kouvel - Fisher methods, critical parameters of the $Ni_{45}Co_5Mn_{31}Al_{19}$ ribbon were determined to be $T_C \approx 290$ K, $\beta \approx 0.58$, $\gamma \approx 0.92$ and $\delta \approx 2.59$. The obtained values of the critical exponents indicate that the magnetic order of the alloy ribbon is close to the mean-field model.

1. Introduction

The magnetocaloric effect (MCE) is an intrinsic property of the magnetic material. Basically, magnetocaloric effect is the conversion of magnetic energy into heat energy when the material is exposed in changing magnetic field. This effect appears at all materials with different intensities and is assessed by the magnetic entropy change (ΔS_m) and adiabatic temperature variation (ΔT_{ad}). MCE has been widely utilized in magnetic materials to reach low temperatures. Recently, the giant magnetocaloric effect (GMCE) at room temperature has attracted the attention of researchers by application potential for magnetic refrigeration [1 - 5].

Among magnetocaloric materials, an interesting class is Ni–Mn based Heusler alloys. The Ni-Mn based alloys have been shown to exhibit large magnetocaloric effects, such as providing both the negative and positive magnetocaloric effects. Besides that, the shape memory effect and other interesting properties were also observed [6 - 9]. In the Ni-Mn-Al Heusler alloys, the Neel temperature $T_N \approx 300$ K was found to be virtually independent of composition [10]. The Ni-Mn-Al alloys with theirs relatively low cost and high ductility is a potentially attractive candidate material as a magnetic refrigerant.

Recently, it was reported that Co doping had a strong effect on the magnetic phase transformation of materials. Partial substitution of Co for Ni in the alloys leads to the significant increase of the magnetization change at the martensitic transformation (ΔM) which greatly enhanced the MCE [11-13]. The martensite-austenite temperature decreases gradually, while the Curie temperature increases greatly with increasing the Co concentration. Substitution of Co for Ni will reinforce the magnetic exchange interactions and the ferromagnetic phase of alloys [14-17]. However, the magnetic phase transitions and MCEs of the (Ni,Co)-Mn-Al bulk alloys are very sensitive to crystallize structure and it normally takes a long time (several days) to make structure stable [18-20]. Comparing the ribbon samples with bulk samples of the same composition, they have different structure and magnetic properties. Specifically, martensitic transformation temperature in $Ni_{50-x}Co_xMn_{31+y}Al_{19-y}$ (x = 5, 10) ribbon alloys is significantly lower bulk alloys. As compared to a weakly magnetic of the $Ni_{50}Mn_{31}Al_{19}$ ribbon, the $Ni_{50-x}Co_xMn_{31+y}Al_{19-y}$ (x = 5, 10) ribbons demonstrate ferromagnetic properties. The $Ni_{45}Co_5Mn_{32}Al_{18}$ ribbon was found to exhibit a well-defined martensitic-austenitic phase transition [20-23].

In this work, we investigated magnetic, magnetocaloric and critical properties of $Ni_{50-x}Co_xMn_{50-y}Al_y$ (x = 5 and 10; y = 17, 18 and 19) rapidly quenched ribbons.

2. Experiment

Six alloy ingots with nominal compositions of $Ni_{50-x}Co_xMn_{50-y}Al_y$ (x = 5 and 10; y = 17, 18 and 19) were prepared from pure elements (99.9%) of Ni, Co, Mn and Al

* Corresponding author: yennh@ims.vast.ac.vn

by using arc-melting method in Argon gas. Melt-spinning method was then used to fabricate the alloy ribbons with tangential velocity of copper wheel of 40 m/s. The thickness and width of the ribbons are about 20 μm and 1.5 mm, respectively. The structure of the alloys was investigated by powder X-ray diffraction (XRD) method. The magnetic properties and magnetocaloric effect of the alloys were characterized on a vibrating sample magnetometer.

3. Result and discussion

XRD patterns of the $Ni_{50-x}Co_xMn_{50-y}Al_y$ (x = 5 and 10; y = 17, 18 and 19) ribbons measured at room temperature are shown in figure 1. Structural analyses revealed that besides the main phase associated with an austenitic $L2_1$ structure (space group: Fm3m), some XRD peaks with low intensity corresponding to martensitic 10*M* (space group: Pmma) phase is also present. With high concentration of Al, the 10*M* phase develops strongly in the alloy ribbons. It should be noted that, a small change of structure in this kind of materials can greatly affect on magnetic properties of the ribbons as presented below.

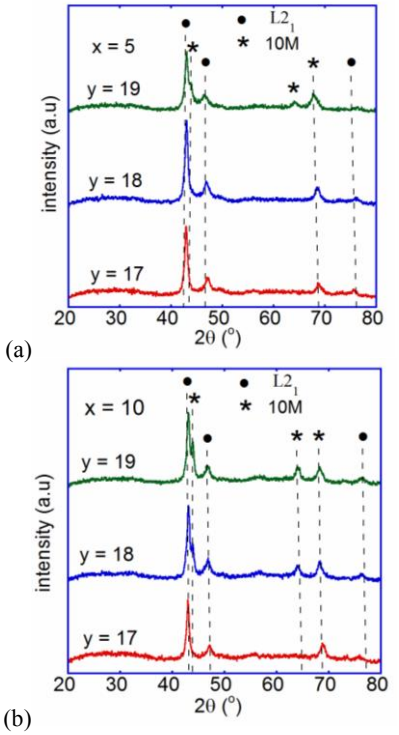

Fig. 1. *XRD patterns of $Ni_{50-x}Co_xMn_{50-y}Al_y$ ribbons with x = 5 (a) and x = 10 (b).*

The magnetic properties of the samples were characterized by the magnetization measurements (figure 2). The results show that all the samples with Co-concentration of 10 at% behave as the soft magnetic material with a low coercivity less than 20 Oe (figure 2a). The temperature dependence of magnetization, $M(T)$, for the ribbons in the field 100 Oe are showed in figure 2 (b). One can see that the shape of thermomagnetization curves considerably depend on both the concentrations of Co and Al. As for examples, the magnetization of the samples with x = 5 is increased from ~ 0.1 emu/g (for y = 17) to ~ 4.7 emu/g (for y = 19). In addition, the $Ni_{45}Co_5Mn_{31}Al_{19}$ and $Ni_{40}Co_{10}Mn_{33}Al_{17}$ ribbons reveal both the first-order (FOPT) and second-order (SOPT) magnetic phase transition. While the FOPT is strongly influenced by Al-concentration, the SOPT (FM-PM) is almost unchanged. By increasing the Co-concentration from 5 at% to 10 at%, the Curie temperature (T_C) is strongly increased from ~ 290 K (for x = 5 and y = 19) to ~ 393 K (for x = 10 and y = 19). The magnetization of the alloy ribbons is also increased considerably with the Co-concentration.

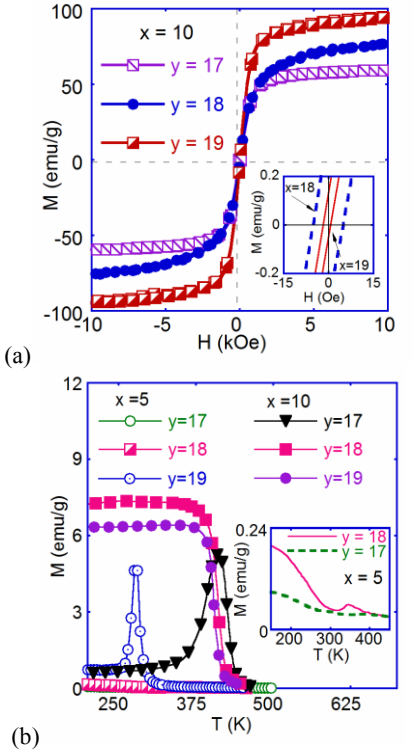

Fig. 2. *M(H) loops at room temperature (the inset enlarges the typical loops at low magnetic field) (a), M(T) curves measured in magnetic field of 100 Oe (the inset enlarges M(T) curves at low magnetization) (b) of $Ni_{50-x}Co_xMn_{50-y}Al_y$ (x = 5 and 10; y = 17, 18 and 19) ribbons.*

The different influence of Co and Al on T_C can be explained by the dependence of T_C on the exchange interaction in the materials. The ferromagnetic exchange interaction between Ni and Mn atoms in the (Ni,Co)-Mn-Al alloys essentially decides value of their T_C [24, 25]. Partial substitution of Mn by Al (paramagnetic material) hardly affects the exchange interaction of Ni and Mn atoms. But the substitution of Ni by Co (ferromagnetic material) enhances the exchange interaction of the alloy resulting in the large change of T_C. As compared to the $Ni_{45}Co_5Mn_{31}Al_{19}$ bulk alloy with annealing at 1370 K for 24 h, martensite transformation temperature in ribbon is significantly higher, while Curie temperature is almost unchanged [20].

Among this series, the $Ni_{45}Co_5Mn_{31}Al_{19}$ sample shows two strong magnetic phase transitions near room temperature region. Therefore, it was chosen as a representative one for analyzing magnetic properties. For further understanding the type of the phase transition and MCE of the alloy ribbons, the isothermal magnetization curves, $M(H)$, with magnetic field up to 13.5 kOe were performed. Figure 3a shows $M(H)$ curves at various temperatures of the $Ni_{45}Co_5Mn_{31}Al_{19}$ sample.

The magnetic orders in a second-order magnetic phase transition of the material can be additionally understood by determining the critical parameters upon using Arrott plots [26]. The Arrott plots, H/M versus M^2 (figure 3b), were constructed from $M(H)$ data. The $M^2 - H/M$ curves are non-linear at low magnetic field and linear at high magnetic field. Values of the spontaneous magnetization (M_S) and the inverse initial susceptibility (χ_0^{-1}) at different temperatures were derived from Arrott plots.

The critical parameters of β, γ and δ relate to the two above quantities by following equations [26, 27]:

$$M_S(T) = M_0(-\varepsilon)^{\beta} \qquad \varepsilon < 0 \qquad (1)$$

$$H = DM^{\delta} \qquad \varepsilon = 0 \qquad (2)$$

$$\chi_0^{-1}(T) = \frac{H_0}{M_0}\varepsilon^{\gamma} \qquad \varepsilon > 0 \qquad (3)$$

$$\delta = 1 + \gamma / \beta \qquad (4)$$

where M_0, H_0 and D are the critical amplitudes and $\varepsilon = (T - T_C)/T_C$ is the reduced temperature.

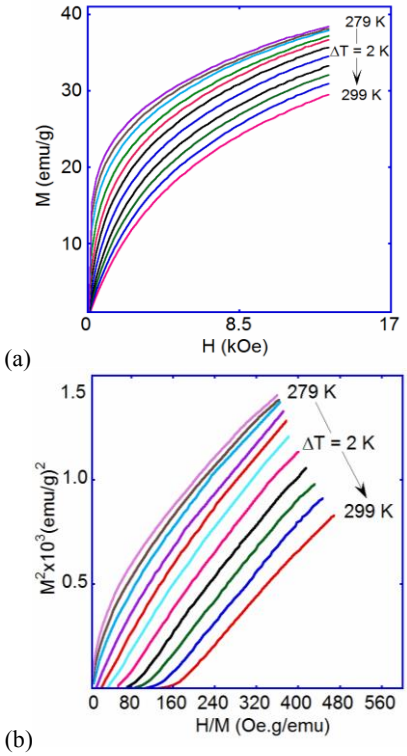

Fig. 3. *Isothermal magnetization curves around T_C (a) and Arrott plots (b) for $Ni_{45}Co_5Mn_{31}Al_{19}$ ribbon.*

The linear extrapolation from high field to the intercepts with the M^2 and H/M axes gives the values of $M_S(T)$ and $\chi_0^{-1}(T)$, respectively. The critical parameter T_C, β and γ obtained from fitting $M_S(T)$ and $\chi_0^{-1}(T)$ data (figure 4a) by using the according formulas (1) and (3), while δ was calculated by using the Widom scaling relation, equation (4) [27, 28]. As resulted, the $Ni_{45}Co_5Mn_{31}Al_{19}$ ribbon possesses $T_C \approx 290$ K, $\beta \approx 0.59$, $\gamma \approx 0.92$ and $\delta \approx 2.56$. The critical parameters are quite close to mean-field theory ($\beta = 0.5$, $\gamma = 1$ and $\delta = 3$) [28].

Alternatively, the critical parameters can be obtained more accurately by the Kouvel - Fisher method [29]. Similarity with Arrott – Noakes method, $M_S(T)$ and $\chi_0^{-1}(T)$ are determined by plotting $M^{1/\beta}$ versus $(H/M)^{1/\gamma}$ curves. The critical parameters of β and γ relate to the two above quantities by these equations:

$$M_S(T)\left[dM_S/dT\right]^{-1} = (T - T_C)/\beta \qquad (5)$$

$$\chi_0^{-1}(T)\left[d\chi_0^{-1}(T)/dT\right]^{-1} = (T - T_C)/\gamma \qquad (6)$$

Again, the critical parameters T_C, β and γ obtained from fitting $M_S(T)$ and $\chi_0^{-1}(T)$ data by using the according formulas (5) and (6). Figure 4b shows Kouvel-Fisher curves of the $Ni_{45}Co_5Mn_{31}Al_{19}$ ribbon with fitting results of $T_C \approx 291$ K, $\beta \approx 0.58$ and $\gamma \approx 0.92$. Basing on the formula (4), the δ value was calculated to be 2.59. One can see that the critical parameter values determined from the Kouvel-Fisher method are in good agreement with those obtained by the Arrott-Noakes fittings.

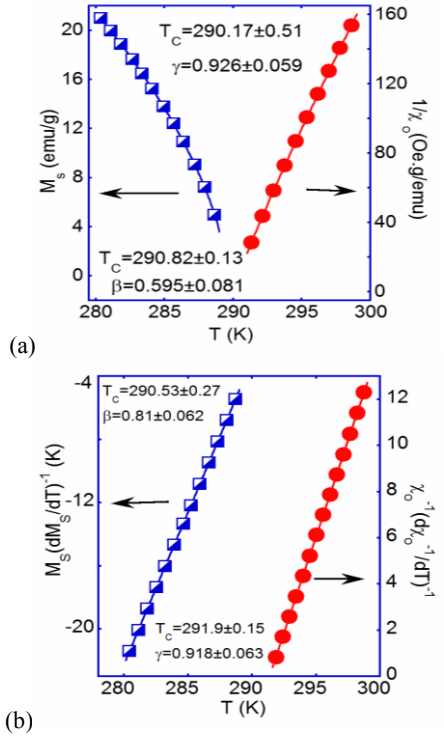

Fig. 4. *$M_S(T)$ and $\chi_0^{-1}(T)$ along with fittings to Arrott-Noakes relations (a) and Kouvel-Fisher plots (b) for $Ni_{45}Co_5Mn_{31}Al_{19}$ ribbon.*

Assessing the reliability of the critical parameters can be carried out by using the static-scaling theory [28, 30]. The isothermal magnetization is determined by the formula:

$$M(H,\varepsilon) = \varepsilon^{\beta} f_{\pm}(H|\varepsilon|^{-(\beta+\gamma)}) \qquad (7)$$

Where f_+ and f_- are regular functions for temperatures $T > T_C$ and $T < T_C$, respectively.

Figure 5 shows the static-scaling plots of $M|\varepsilon|^{-\beta}$ versus $H|\varepsilon|^{-(\beta+\gamma)}$ in the log scale with the obtained critical parameters. We can see that points of the data fall on two universal branches with $T > T_C$ and $T < T_C$. Consequently, the critical values in our study are reliable results.

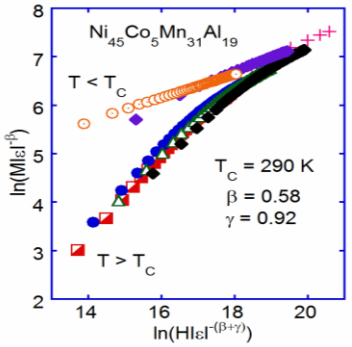

Fig. 5. *The static-scaling performances for $Ni_{45}Co_5Mn_{31}Al_{19}$ ribbon.*

Magnetocaloric effect in the alloys was assessed by the magnetic entropy change (ΔS_m). This value was calculated basing on the isothermal magnetizations (figure 3a). Fig 6 shows $\Delta S_m(T)$ curves of the $Ni_{45}Co_5Mn_{31}Al_{19}$ ribbon under several magnetic field change (ΔH = 2, 6, 10 and 13.5 kOe). With ΔH = 13.5 kOe, the maximum magnetic entropy change are about 2

and -1 J·kg^{-1}·K^{-1} for negative and positive magnetocaloric effects, respectively. These results are similar to reports by Y. Kim et al [18, 19]. In addition, the $|\Delta S_m|_{max}$ value increases with increasing the magnetic field (the above inset of figure 6).

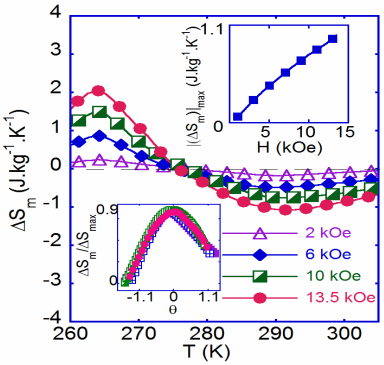

Fig. 6. *Magnetic entropy change (ΔH = 2, 6, 10 and 13.5 kOe) versus temperature for $Ni_{45}Co_5Mn_{31}Al_{19}$ ribbon. The above inset shows field dependences of $|\Delta S_m|_{max}$ at $T \approx T_C$. The below inset shows universal master curves of $\Delta S_m / \Delta S_{max}$ versus θ.*

The temperature dependence of ΔS_m under different applied field for the second-order phase transition of materials can be described by the universal master curves [31, 32]. Basing on the $\Delta S_m(T)$ curve, the $\Delta S_m / \Delta S_{max}$ versus θ plots are constructed. White θ value is determined by the formula:

$$\theta = \begin{cases} -(T - T_C)/(T_{r1} - T_C), & T \le T_C \\ (T - T_C)/(T_{r2} - T_C), & T > T_C \end{cases} \quad (8)$$

Where T_{r1} and T_{r2} are the temperature of the two reference points. For the present study, they are selected as those corresponding to $\Delta S_m(T_{r1,2}) = k.\Delta S_{max}$ $(k = 0.5)$. This choice of k does not affect the actual construction of the universal curve, as it implies only proportionality constant. The below inset of figure 6 shows the universal master curve of the $Ni_{45}Co_5Mn_{31}Al_{19}$ ribbons. All $\Delta S_m(T)$ data under different applied fields are collapsed into a universal master curve. This is an interesting property of the second-order phase transition of materials.

4. Conclusion

Structure of the $Ni_{50-x}Co_xMn_{50-y}Al_y$ (x = 5 and 10; y = 17, 18 and 19) ribbons exhibits multi-crystalline phases of the $L2_1$ and 10M types. All the alloy ribbons behave as the soft magnetic materials and their Curie temperature strongly increases with increasing the Co-concentration and hardly changes with increasing the Al-concentration. The maximum magnetic entropy change with variation of magnetic field of 13.5 kOe for the $Ni_{45}Co_5Mn_{31}Al_{19}$ ribbon is about 2 and -1 J·kg^{-1}·K^{-1} for negative and positive magnetocaloric effects, respectively. Critical parameters of the alloy are close to those of the mean-field model for long-range ferromagnetic orders.

This work was supported by Vietnam Academy of Science and Technology under grant No. VAST.HTQT.NGA.05/17-18 and Russian Foundation for Basic Research under grant № 17-58-540002. A part of the work was done in Key Laboratory for Electronic Materials and Devices and Laboratory of Magnetism and Superconductivity, Institute of Materials Science, Vietnam.

References

1. O. Tegus, E. Brück, K.H. Buschow, F.R. Boer, Nature. **415,** 6868 (2002).
2. X. Zhang, B. Zhang, S. Yu, Z. Liu, W. Xu, G. Liu, Phys. Rev. B **76,** 132403 (2007).
3. E. Bruck, J. Appl. Phys **38**, 381 (2005).
4. Y.B. Yang, X.B. Ma, X.G. Chen, J.Z. Wei, R. Wu, J.Z. Han, H.L. Du, C.S. Wang, S.Q. Liu, Y.C. Yang, Y. Zhang, J.B. Yang, J. Appl. Phys. **111**, 07A916 (2012).
5. K.A. Gschneidner, V.K. Pecharsky, Int. J. Ref. **31**, 945 (2008).
6. V.K. Pecharsky, K.A. Gschneidner, A.O. Pecharsky, A.M. Tishin, Phys. Rev. B **64**, 144406 (2001).
7. T. Krenke, E. Duman, M. Acet, E.F. Wassermann, X. Moya, L. Mañosa, Nat. Mater. **4**, 450 (2005).
8. A. Planes, L. Mañosa, M. Acet, J. Phys. **21**, 233201 (2009).
9. R. Kainuma, W. Ito, R.Y. Umetsu, K. Oikawa, K. Ishida, Appl. Phys. Lett. **93**, 091906 (2008).
10. S. Morito, T. Kakeshita, K. Hirata, K. Otsuka, Acta Mater. **46**, 5377 (1998).
11. P. Felcher, J. Cable, K. Wilkinsonm, J. Phys. Chem. Solids **24**, 1663 (1963).
12. F. Gejima, Y. Sutou, R. Kainuma, K. Ishida, Metall. Mater. Trans. A **30**, 2721 (1999).
13. H.C. Xuan, F.H. Chen, P.D. Han, D.H. Wang, Y.W. Du, Intermetallics **47**, 31-35 (2014).
14. M.V. Lyange, E.S. Barmina, V.V. Khovaylo, Mater. Sci. Forum **81**, 232-242 (2015).
15. C. Liu, W. Zhang, Z. Qian, Z. Hu, Q. Zhao, Y. Sui, W. Su, M. Zhang, Z. Liu, G. Liu, G. Wu, J. Alloys Comp. **433**, 37 (2007).
16. A.C. Paduani, A. Migliavacca, M.L. Sebben, J.D. Ardisson, M.I. Yoshida, S. Soriano, M. Kalisz, Solid State Commun. **141**, 145 (2007).
17. T. Busgen, J. Feydt, R. Hassdorf, S. Thienhaus, M. Moske, Phys. Rev. B **70**, 014111 (2004).
18. Y. Kim, W.B. Han, H.S. Kim, H.H. An, C.S. Yoon, J. Alloys Compd. **557**, 265 (2013).
19. Y. Kim, S.J. Lee, W.B. Han, H.-S. Kim, H.H. An, C.S. Yoon, J. Appl. Phys. **113**, 17B102 (2013).
20. X. Xu, W. Ito, M. Tokunaga, R.Y. Umetsu, R. Kainuma, K. Ishida, Mater. Trans. **51**, 1357 (2010).
21. M.V. Lyange, V. Khovaylo, R. Singh, S.K. Srivastava, R. Chatterjee, L.K. Varga, J. Alloys Compd. **586**, 218 (2014).
22. V. Khovaylo, M. Lyange, K. Skokov, O. Gutfleisch, R. Chatterjee, X. Xu, R. Kainuma, Mater. Sci. Forum **738**, 446 (2013).
23. X. Xu, W. Ito, T. Kanomata, R. Kainuma, Entropy **16**, 1808 (2014).
24. J. Rusz, L. Bergqvist, J. Kudrnovský and I. Turek, Phys. Rev. B **73**, 214412 (2006).
25. D.T. Huu, N.H. Yen, P.T. Thanh, N.T. Mai, T.D. Thanh, T.L. Phan, S.C. Yu, N.H. Dan, J. Alloys Compd. **622**, 535 (2015).
26. A. Arrott, J.E. Noakes, Phys. Rev. Lett. **19**, 786 (1967).
27. B. Widom, J. Chem, Phys. **41**, 1633 (1964).
28. H.E. Stanley, *Introduction to phase transitions and critical phenomena* (Oxford University Press, 1971).
29. J.S. Kouvel, M.E. Fisher, Phys. Rev. **136**, A1626 (1964).
30. S.K. Banerjee, Phys. Lett. **12**, 16 (1964).
31. V. Franco, J.S. Blazquez, A. Conde, Appl. Phys. Lett. **89**, 2 (2006).
32. V. Franco, A. Conde, Int. J. Ref. **33**, 3 (2010).